X-Ray Computed Tomography (XRCT)

The recent development in image analysis techniques and software has provided the chance to use techniques such as XRCT in a wide range of applications. It can be utilised with particular software for characterising concrete microstructures including air pores (porosity) and aggregate distribution, whether it is mineral and/ or alternative. XRCT is a non-destructive technique that can obtain cross-sectional images of the assessed sample and the computer processes the results, displaying them as 2D images. 3D images can be reconstructed using stacks of the 2D images within supplementary software. The processes described above are summarised in Figure .خطأ! لا يوجد نص من النمط المعين في المستند-1[128].

Thescan is carried out by passing x-rays through a solid body/material (see Figure خطأ! لا يوجد نص من النمط المعين في المستند-2) while it is rotating where the scan starts from the top down to the bottom, as seen in Figure .خطأ! لا يوجد نص من النمط المعين في المستند-1. The x-rays are detected after they have passed through the body and their intensity is measured, e.g. beams that have passed through less dense constituents are much less attenuated than those that have passed through high density solid matter. A computer is used to reconstruct this information where the relative density of the constituents is represented according to grey scale contrast on the image, e.g. high density/ x-ray attenuation is represented by brighter pixels and low density by darker pixels. XRCT can be used for studying/evaluating concrete quality including the distribution, shape, orientation and size of key features such as aggregates and pores, as well as crack length and propagation [129].

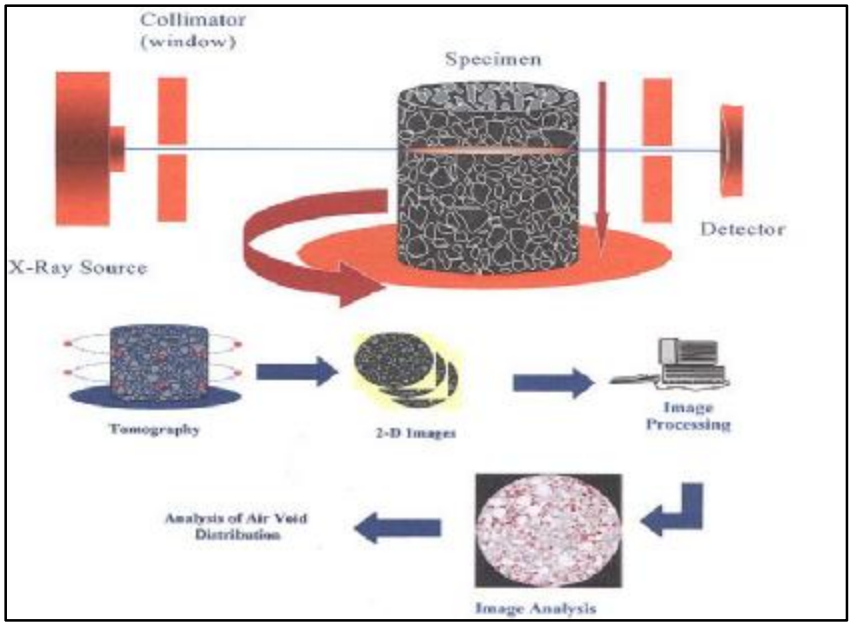

Figure .خطأ! لا يوجد نص من النمط المعين في المستند-1: Example XRCT scan and sequence of image analysis techniques [129]

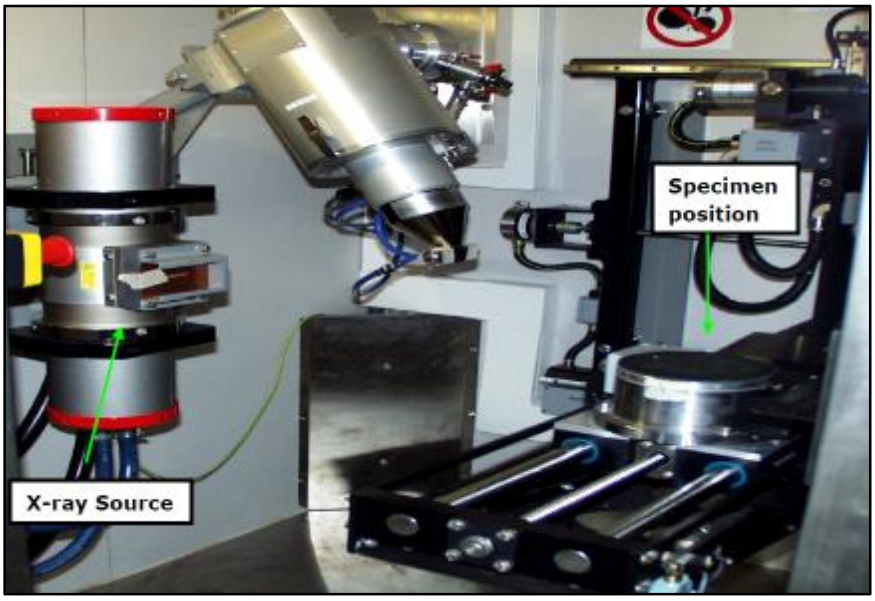

Figure .خطأ! لا يوجد نص من النمط المعين في المستند-2: XRCT system [128]

In this study, in order to examine the effect of pre-coating/treating methods on the macro-scale (rounded) porosity caused by entrapment, XRCT was conducted using a Phoenix Nanotom 180NF XRCT system (see Figure .**خطأ!** لا يوجد نص من النمط المعين في المستند-3; GE Sensing and Inspection Technologies, GmbH, Wunsdorf, Germany) with a maximum electron acceleration energy of 110 kV, and acquiring 1440 projection images. During the scan the detector size was set to provide a spatial resolution of 34.6 μm and the scan length was approximately 45 min per sample.Images were reconstructed, after each set of projections, using the back

projection algorithm in the ‘datos|x rec’ software. No corrections were required for beam hardening or sample displacement artefacts. All post-scanning image analysis was conducted using ImageJ software v1.44p.

Figure .خطأ! لا يوجد نص من النمط المعين في المستند-3: X-Ray Computed Tomography (XRCT) Phoenix Nanotom 180NF XRCT system

The tested sample was a 30 mm diameter cylinder (see Figure .خطأ! لا يوجد نص من النمط المعين في المستند-3B) cored from a ≥28-day-old 100 mm water-cured cubic sample and air-dried under laboratory conditions (22°C ± 2 and 65% RH ± 5) before being wrapped in a nylon sheet prior to scanning. Infranview image software was used toinitially convert all X-ray images to 8-bit greyscale before scaling to 34.6 μm resolution. In order toeliminate any potential edge effects, only the middle 540 images in the stack were taken and the remaining 172 images at the top and bottom were removed. The images were then cropped into a 28 mm diameter cylinder to minimise edge effects by applying the ‘clear outside’ edit feature. The brightness/contrast was manually adjusted to bracket the upper/lower limits of the greyscale histogram before applying a 1-px median filter followed by one pass of the despeckle noise filter. The brightness/contrast was then re-adjusted to bracket the upper/lower limits of the new histogramfollowed by applying the ‘default’ thresholding algorithm, as shown in Figure **.خطأ! لا يوجد نص من النمط المعين في المستند**-4, where the peaks 1, 2 and 3 of the greyscale histogram correspond to the air voids, rubber particles and natural aggregate/cement matrix respectively.

It is worthwhile to note that only pores with diameter ≥*c.* 100 μm could be identified due to the limitations of the scan resolution (see Figure **.خطأ! لا يوجد نص من النمط المعين في المستند**-4 A), and all of these were

identified as entrapped air voids distributed within the matrix as opposed to interfacial voids occurring at the periphery of the aggregates. This can be seen from 3D visualisation of the air void and rubber aggregate distribution within a representative core sample of $SCRC_2$ (see Figure **خطأ! لا يوجد نص من النمط المعين في المستند.**-4B), which was achieved using VGStudio Max 2.0 464-bit software, VGL version 4.0 (2009). To determine the pore size distribution the threshold could simply be set after the first peak (see Figure **خطأ! لا يوجد نص من النمط المعين في المستند.**-4A), before applying the binary fill-holes filter in order to remove white pixel noise from the core of individual voids. The scale was set to 0.0289 pixels/μm, and then the measurements of pore area and standard deviation were taken and plotted using Microsoft Excel.

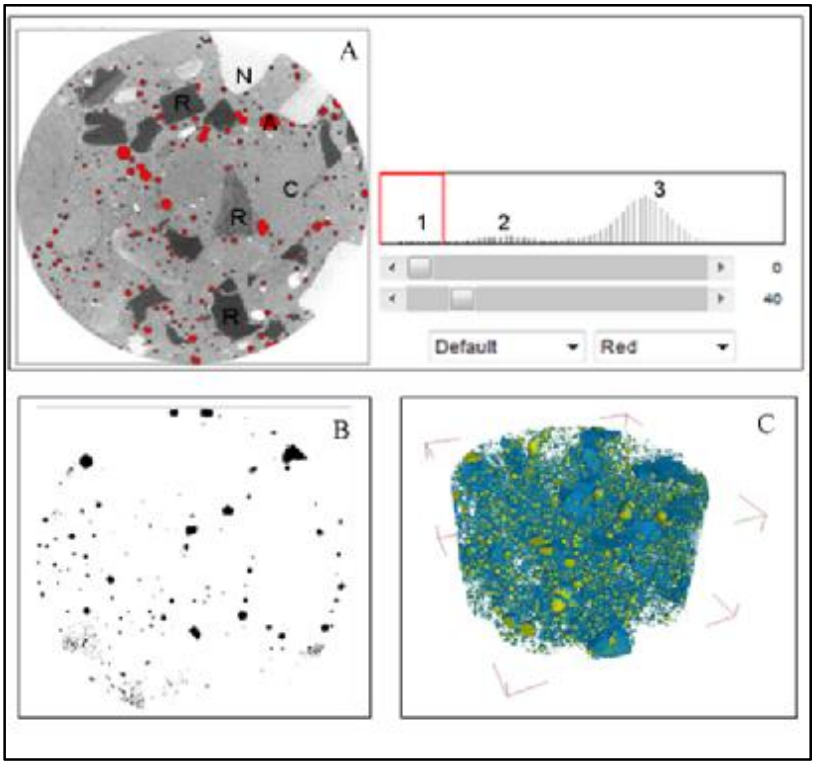

Figure **خطأ! لا يوجد نص من النمط المعين في المستند.**-4: (A) threshold sample where R = rubber aggregate, N = natural aggregate, A = air voids and C = cement paste. (B) Binary thresholded image and (C) Corresponding 3D reconstruction where yellow represents air voids and blue represents rubber particles.

3.1.1 Scanning Electronic Microscopy (SEM)

Principles of SEM

SEM is a microscopic imaging technique that uses a high energy electron beam to scan a specimen under vacuum. Electrons are accelerated down a column towards the sample at energies ranging from a few hundred to tens of thousands of electron volts. When the beam leaves the column, it is deflected using scan

coils into a scanning pattern that is focused to a spot on the sample (see Figure خطأ! لا يوجد نص من النمط المعين في المستند.-5). SEM can use different analysis techniques involving the secondary electron (SE) detector, back-scattered electron (BSE) detector, and Energy Dispersive X-ray Spectroscopy (EDS). In SE detection mode, the SEM can provide very high-resolution images of sample surface morphology down to nano scale resolution. This is obtained by analysing the signals resulting from the interactions between the electron beam and atoms at or near the surface of the sample. SEM micrographs usually reveal the surface structure of the tested sample (surface morphology) as they have a large depth of field yielding a characteristic three-dimensional appearance due to the very narrow convergence angle of the electron beam. SE can provide a wide range of magnifications from 10 times to more than 5×10^5 times [165].

Back-scattered electrons (BSE) are reflected from just beneath the sample surface by elastic scattering, and are commonly used in analytical SEM along with the spectra from EDS analysis. BSE micrographs can provide information about the distribution of different elements in the sample due to the strong relation between the intensity of the BSE signal and the atomic number of the specimen, i.e. high atomic number samples produce higher contrast/appearance up to 5-10 nm. Characteristic X-rays are emitted when the electron beam ejects an inner shell electron from the sample, causing a higher-energy electron to fill the shell and release residual energy in the form of photons at x-ray wavelength. The energy of these characteristic X-rays are used to identify the elemental composition and their spatial distribution across a flat (polished) sample surface [166].

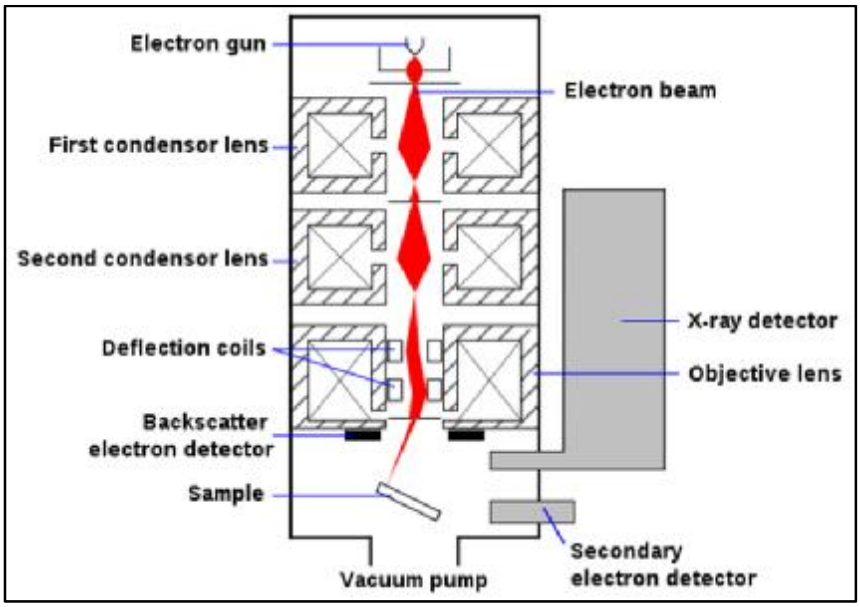

Figure .خطأ! لا يوجد نص من النمط المعين في المستند-5: Schematic diagram of an SEM [166]

Scanning process and image formation

Typical electron guns are usually fitted with a W (Tungsten) filament or LaB_6 (Lanthanum Hexaboride) cathode. Tungsten is often used in thermionic electron guns because it has the highest melting point and lowest vapour pressure of all metals, thereby allowing it to be heated for electron emission, and modest cost. Other types of electron emitters include Field Emission Guns (FEG), which may be of the cold-cathode type using tungsten single crystal emitters or the thermally assisted Schottky type. The electron gun/FEG, that produce the electron beam as shown in Figure .خطأ! لا يوجد نص من النمط المعين في المستند-5, typically operate at an accelerating voltage of between 0.2 kV to 40 kV. The beam is focused by one or two condenser lenses to a spot ranging between 0.4 nm to 5 nm in diameter. The scan is carried out by passing the beam through pairs of scanning coils or pairs of deflector plates in the electron column, typically in the final lens, which deflect the beam in the x and y axes so that it scans in a raster fashion over a rectangular area of the sample surface.

Once the electron beam interacts with the sample, the electrons lose energy by repeated random scattering and absorption within a teardrop-shaped volume of the specimen known as the interaction volume, which extends from less than 100 nm to around 5 µm into the surface. The size of the interaction volume depends on the electron's landing energy, the atomic number of the specimen and the specimen's density. The energy exchange between the electron beam and the sample results in the reflection of high-energy electrons by elastic scattering, emission of secondary electrons by inelastic scattering and the emission of electromagnetic radiation, each of which can be detected by specialized detectors. The beam current absorbed by the specimen can also be detected and used to create images of the distribution of specimen current. Electronic amplifiers of various types are used to amplify the signals, which are displayed as variations in brightness on a computer monitor Each pixel of computer video-memory is synchronised with the position of the beam on the specimen in the microscope, and the resulting image is therefore a distribution map of the intensity of the signal being emitted from the scanned area of the specimen [167, 168]

In order to study the effect of the P-C/T methodologies on the microstructure of PRC and SCRC including the ITZ micro-porosity and other features, and the bonding characteristics between the rubber particles and the cement paste, a microstructural analysis was carried out. For this purpose,a Philips XL30 Environmental SEM (Figure .خطأ! لا يوجد نص من النمط المعين في المستند-6) with Field Emission Gun (ESEM-FEG) equipped SEM was used along with an Oxford Instruments Inca model Energy Dispersive X-Ray spectrometer (EDS) with 133-eV resolution of the MnK_α peak at Full Width Half Maximum (FWHM). The obtained micrographs were recorded using an Everhart-Thornley type Secondary Electron (SE) detector and a Back Scattered Electron (BSE) detector supplied by K. E. Developments used in high vacuum (hivac) SEM mode.

Figure .خطأ! لا يوجد نص من النمط المعين في المستند-6: Philips XL30 Environmental SEM

The scanned samples were taken from the end-third of failed flexural test prisms from the same positions in order to reduce the possibility of post-yield damage and to be representative to a high extent. Samples were prepared by fracture cross section followed by vacuum cold-mounting in epoxy resin. The cross sectional surface was then polished with wet SiC polishing wheels (P240, P400, P800, P1200) before washing with industrial methylated spirit (IMS), followed by further polishing with 6 µm and then 1 µm diamond paste. Polished samples were Pt sputter coated in order to provide high-resolution imaging whilst still allowing light element EDS analysis, as shown in Figure .خطأ! لا يوجد نص من النمط المعين في المستند-7.

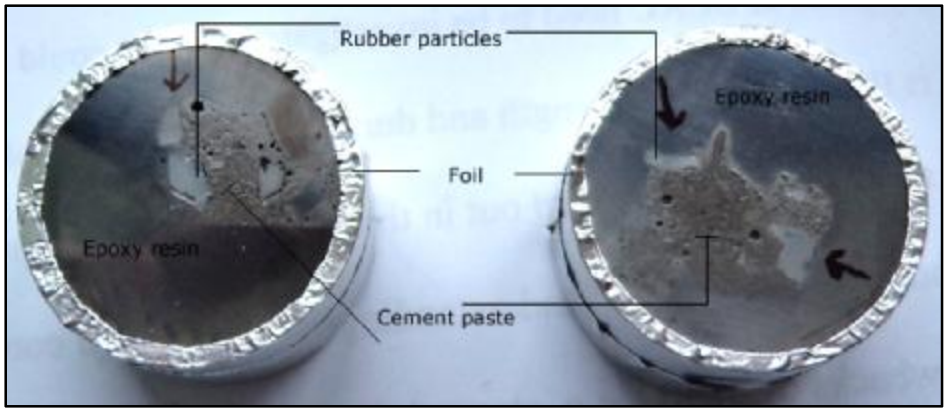

Figure .خطأ! لا يوجد نص من النمط المعين في المستند-7: Scanned cross-section resin-mounted ITZ samples

The ImageJ software tool v1.44p was used to analyse five representative micrographs that were randomly taken for each sample in order to statistically quantify the width of interfacial gap void formation (due to de-bonding). Ten measurements were recorded for each image such that the mean interfacial gap void width is the average of 50 readings. The interfacial gap voids were identified by thresholding using the same thresholding algorithm as was applied for the XRCT analysis previously mentioned (see section 3.2.5)